



HAL
open science

Thiol-Poly(Sodium Styrene Sulfonate) (PolyNaSS-SH) Gold Complexes: From a Chemical Design to a One-Step Synthesis of Hybrid Gold Nanoparticles and Their Interaction with Human Proteins

Céline Falentin-Daudre, Mounia Aitouakli, Jean Sebastien Baumann, Nadia Bouchemal, Vincent Humblot, Veronique Migonney, Jolanda Spadavecchia

► To cite this version:

Céline Falentin-Daudre, Mounia Aitouakli, Jean Sebastien Baumann, Nadia Bouchemal, Vincent Humblot, et al.. Thiol-Poly(Sodium Styrene Sulfonate) (PolyNaSS-SH) Gold Complexes: From a Chemical Design to a One-Step Synthesis of Hybrid Gold Nanoparticles and Their Interaction with Human Proteins. ACS Omega, 2020, pp.8137-8145. 10.1021/acsomega.0c00376 . hal-02571960

HAL Id: hal-02571960

<https://hal.science/hal-02571960v1>

Submitted on 13 May 2020

HAL is a multi-disciplinary open access archive for the deposit and dissemination of scientific research documents, whether they are published or not. The documents may come from teaching and research institutions in France or abroad, or from public or private research centers.

L'archive ouverte pluridisciplinaire **HAL**, est destinée au dépôt et à la diffusion de documents scientifiques de niveau recherche, publiés ou non, émanant des établissements d'enseignement et de recherche français ou étrangers, des laboratoires publics ou privés.

Thiol-Poly(Sodium Styrene Sulfonate) (PolyNaSS-SH) Gold Complexes: From a Chemical Design to a One-Step Synthesis of Hybrid Gold Nanoparticles and Their Interaction with Human Proteins

Céline Falentin-Daudré, Mounia Aitouakli, Jean Sébastien Baumann, Nadia Bouchemal, Vincent Humblot, Véronique Migonney, and Jolanda Spadavecchia*



Cite This: *ACS Omega* 2020, 5, 8137–8145



Read Online

ACCESS |



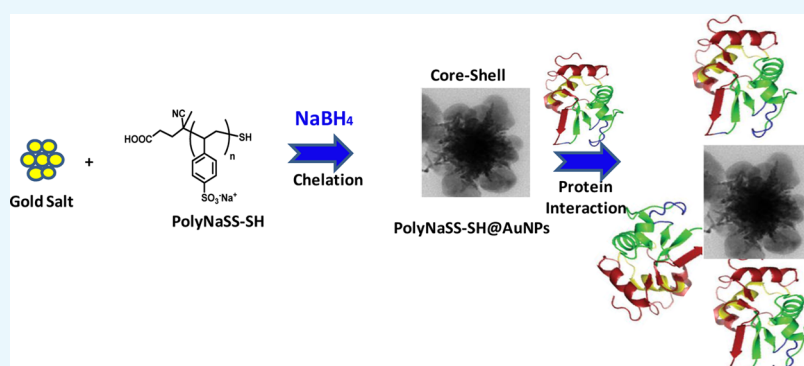
Metrics & More



Article Recommendations



Supporting Information



ABSTRACT: This study highlights recent advances in the synthesis of nanoconjugates based on gold (Au(III)) complex with a bioactive polymer bearing sulfonate groups called thiol-poly(sodium styrene sulfonate) (PolyNaSS-SH) with various molecular weights (5, 10, and 35 kDa). The three nanomaterials differ substantially in shape and structure. In particular, for PolyNaSS-SH of 35 kDa, we obtained a characteristic core–shell flower shape after chelation of the Au(III) ions and successively reduction with sodium borohydride (NaBH₄). The mechanism of formation of the hybrid nanoparticles (PolyNaSS-SH@AuNPs (35 kDa) and their interactions between plasmatic proteins (human serum albumin (HSA), collagen I (Col 1), and fibronectin (Fn)) were deeply studied from a chemical and physical point of view by using several analytical techniques such as Raman spectroscopy, UV–visible, transmission electron microscopy (TEM), ¹H NMR, and X-ray photoelectron spectroscopy (XPS).

1. INTRODUCTION

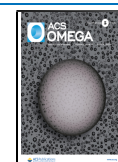
Hybrid gold nanomaterials have received more attention in several fields due to their (i) strong optical absorption in the visible region,¹ (ii) catalytic properties,² and (iii) enhanced sensitivity in surface-enhanced Raman scattering (SERS) studies.³ Despite the fact that gold nanoparticles (AuNPs) can be synthesized to assure functional properties, potential toxicity cannot be predicted by physicochemical properties. There are generally accepted tendencies, for example, that on polyhedral NPs, but are more toxic.⁴ Modification of the NP surface chemistry by coating may modify the effective size of NPs, particularly in case of agglomeration and also their biocompatibility.⁵ The environmentally friendly approach to synthesize AuNPs by using natural macromolecules and biopolymers has been attracting growing interest in the last few years.⁶ Recently, Spadavecchia *et al.* have pioneered a novel simple strategy to synthesize and scale-up hybrid nanoparticles based on biomolecules and/or polymer gold

complex by an experimental approach named “Method IN” in which the polymer or biomolecules interact actively with gold salt (HAuCl₄) by chelation bonding.⁷ This strategy can be applied to any active chemical group that possesses complexation ability, such as carboxylates, phosphonates, and biopolymers.^{8–10} Among these, poly(sodium styrene sulfonate) (PolyNaSS) is considered as a bioactive polymer and was extensively demonstrated to enhance and modulate cell behavior and, more generally, host response. When grafted on implant surfaces, it was shown to substantially improve osteoblast cell adhesion and differentiation *in vitro* and *in vivo*,

Received: January 27, 2020

Accepted: March 12, 2020

Published: April 2, 2020



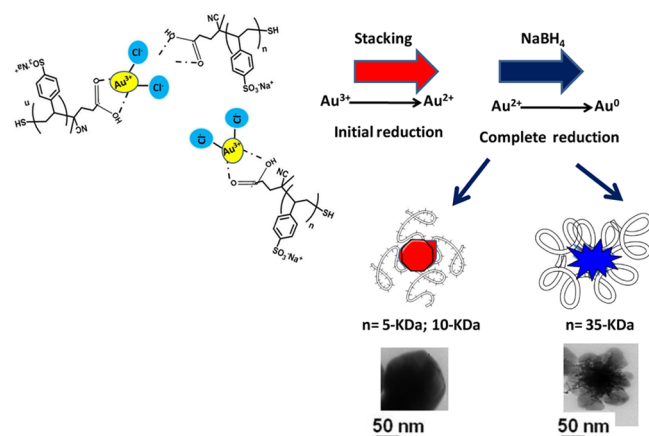
making it as an attractive candidate for application in regenerative medicine.¹¹

The grafting of PolyNaSS can be carried out using radical polymerization from the surface (under heating¹² and UV irradiation^{13,14}) or by using reversible addition–fragmentation chain transfer (RAFT) polymerization onto titanium (Ti) surfaces.^{15,16} For this purpose, Migonney *et al.* have grafted poly(sodium styrene sulfonate) (PolyNaSS) onto titanium surfaces and titanium dioxide nanoparticles (TiO₂NPs) to improve their biological activity.^{15,17} In this work, for the first time, a thiol derivative of poly(sodium styrene sulfonate) (PolyNaSS-SH) was conjugated with AuNPs via the chelation method and investigated for two activities: (i) as a reagent precursor in the chemical synthesis and (ii) as a stabilizer of the AuNPs. In fact, the PolyNaSS-SH/Au interface of the AuNPs enhances the stabilization by steric effects and leads to the formation of a colloidal phase. In addition, the study of the effect of the PolyNaSS-SH molecular weight was accomplished. Indeed, the length of the macromolecular chain of PolyNaSS-SH induces the rapid formation of a core–shell flower AuNP, preventing several chemical step processes. This original core–shell flower shape was tested to check the ability of such nanoparticles to influence the protein interaction with the aim to develop them in the biological field.¹⁸ The understanding of the modulation of protein conformation in the presence of functionalized nanoparticles is a key point to target biomedical applications.¹⁹ Indeed, this was reported in the case of the blood compatibility of implant materials, which was directly associated with processes of serum protein adsorption–desorption on the implant material surface.²⁰ For this purpose, we have investigated and characterized the interactions of PolyNaSS-SH@AuNPs (35 kDa) in the presence of three human proteins as collagen (Col), fibronectin (Fn), and human serum albumin (HSA) present in extracellular matrix (ECM) and blood.

2. RESULTS AND DISCUSSION

2.1. The Formation Mechanism of PolyNaSS-SH@AuNPs. The formation of hybrid gold NPs from PolyNaSS-SH included three steps summarized in Scheme 1:

Scheme 1. Schematic PolyNaSS-SH@AuNPs Reaction during the Growth Process and Zoom of TEM Images Relative to the Shape (Scale Bar, 50 nm)^a



^aPlease note that drawings are not in scale and are not intended to be representative of the full samples composition and stoichiometry.

- (1) Formation of a PolyNaSS-SH-AuCl₄⁻ mixture by gold salt complexation between the terminal carboxylate group (–COO⁻) and sulfonate groups (SO₃⁻) of PolyNaSS-SH.
- (2) First reduction of Au(III) ions by carboxylic acid-terminated PolyNaSS-SH to form Au clusters.
- (3) Complete reduction of metal ions and growth of hybrid gold nanoparticles (PolyNaSS-SH@AuNPs) followed by colloidal stabilization of molecules of PolyNaSS-SH.

Attractive ion–dipole interactions between AuCl₄⁻ ions and a mixture of PolyNaSS-SH molecules ($M_n = 5, 10, \text{ and } 35 \text{ kDa}$) play a key role during the competition process on the Au seed surface during the NP growth process. Based on previous studies,⁸ we assume that, when PolyNaSS-SH was added to the AuCl₄⁻ solution, the PolyNaSS-SH at the molecular weight ($M_n = 5 \text{ or } 10 \text{ kDa}$) was bound to a hybrid complex in a linear conformation followed by a chemical-steric change when the molecular weight increased ($M_n = 35 \text{ kDa}$).

The main difference with previously reported synthetic procedures was that the carboxylic acid terminating PolyNaSS-SH (COOH-PolyNaSS-SH) and all the SO₃⁻ groups exhibited along the macromolecular chains could coordinate Au³⁺ and participate to the stabilization of AuNPs via electrostatic interactions between the terminal carboxylic groups and all the sulfonate groups with chloride auric ions. The final reduction by NaBH₄ completes the growth process to form PolyNaSS-SH@AuNPs with different shapes and sizes. This hypothesis will be explained thanks to the length of macromolecular chains and degree of polymerization in which, at M_n of 35 kDa ($DP_n = 170$), the high number of sulfonate monomer units and the chemical competition between COO⁻ and SO₃⁻ in PolyNaSS-SH favored a growth on crystallographic facet Au [110] and the formation of core–shell of PolyNaSS-SH (35 kDa) onto gold core of nanoparticles (Scheme 1). The higher reactivity of the PolyNaSS-SH (35 kDa) allowed the formation of a slight cross-linked polymer shell embedded on the surface of the AuNPs before the growth of linear polymer chains from the shell.²¹

2.2. Comparative Physicochemical Characterization of PolyNaSS-SH@AuNPs. Three molecular weights of PolyNaSS were synthesized according to the same protocol.

RAFT polymerization allowed synthesizing PolyNaSS with a predetermined molecular weight (5, 10, and 35 kDa). PolyNaSS macromolecules were modified by cleaving the transfer agent to give PolyNaSS-SH. So, the thiol-PolyNaSS (PolyNaSS-SH) used in this study was produced following a two-step strategy. The first step involved the RAFT polymerization of NaSS in solution at 70 °C using 4,4'-azobis(4-cyanovaleric acid) (ACVA) as an initiator, 4-cyano-4-(phenylcarbonothioylthio)pentanoic acid as a chain transfer agent, and water as a solvent.¹⁴

The presence of PolyNaSS-SH chains of different molecular weights on the AuNPs was demonstrated by using Fourier transform infrared (FTIR). The peak's assignments and corresponding positions are given as in Table S1 and Figure S2. The successful grafting of PolyNaSS was confirmed by typical peaks at 2900–3000, 1350–1460, 870, 1010, 1038, and 1130 cm⁻¹, corresponding to $\nu(\text{CH})$ stretching, $\nu(\text{CH})$ deformation, $\nu(\text{C}-\text{C})$ stretching, $\nu(\text{O}-\text{S}-\text{O})$ stretching, SO₃⁻, and aromatic ring, respectively. The presence of PolyNaSS-SH chains of different molecular weights on the AuNPs was also confirmed with ¹H NMR analysis (Figure S3).

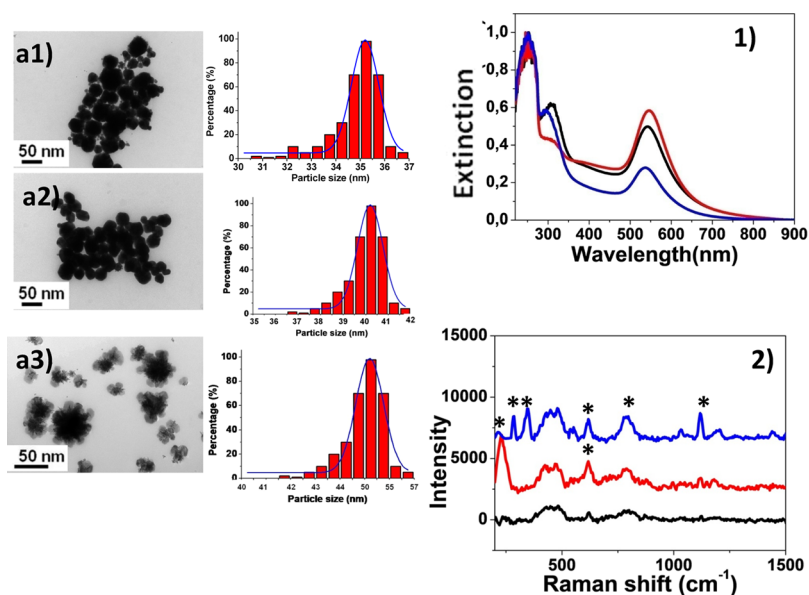


Figure 1. (1) TEM images of PolyNaSS-SH@AuNPs at different molecular weights. (a1) 5, (a2) 10, and (a3) 35 kDa. Scale bars, 50 nm. Normalized UV–vis absorption spectra of PolyNaSS-SH@AuNPs at different molecular weights (5 kDa, black line; 10 kDa, red line; 35 kDa, blue line). (2) Raman spectra of the same PolyNaSS-SH@AuNPs. Experimental conditions: $\lambda_{\text{exc}} = 785 \text{ nm}$; laser power, 20 mW; accumulation time, 180 s.

The grafting of each size of the polymer (5, 10, and 35 kDa) onto AuNPs was observed by typical peaks of polymers at 7.78–7.23 (m, 2H); 6.98–6.08 (m, 2H) corresponding to aromatic CH groups; and 1.99–1.02 (m, 3H), corresponding to $-\text{CH}_2$ and CH groups to the polymer chain (Figures S4 to S9 in the Supporting Information). Several characterizations were carried out by chromatography analysis to confirm the cleavage of the thioester of the PolyNaSS-SH sample whatever its molecular weight (Figures S10 to S12 and Table S2). TEM images corresponding to PolyNaSS-SH@AuNPs with PolyNaSS-SH at 5 and 10 kDa showed a polydispersity of the nanoparticles with an average size of $30 \pm 2 \text{ nm}$ for PolyNaSS-SH@AuNPs (5 kDa) and $35 \text{ nm} \pm 2 \text{ nm}$ for PolyNaSS-SH@AuNPs (10 kDa) (Figure 1a1,a2, respectively). At the opposite, nanostructures with an original core–shell flower-like shape were obtained with PolyNaSS-SH@AuNPs (35 kDa), showing a metal core of around $50 \pm 2 \text{ nm}$ embedded in a shell of polymer of $\pm 20 \text{ nm}$ (Figure 1a3).

The synthesis of flower core–shell gold nanostructures has been reported under specific experimental conditions (chemical reagents and high temperature) or by electrocatalytic methods.²² The stability of the Au–S bonding could be refined by the introduction of multiple thiol-anchoring groups at the polymer chain ends and/or shell cross-linking of polymeric micelles encapsulating AuNPs. Nevertheless, these methods showed several limitations and need a multiple-step organic synthesis.²³ In our case, we demonstrated, for the first time, the possibility of the synthesis of flower-shaped Au core/shell nanoparticles by using PolyNaSS-SH as a stabilizer and complexing agent in aqueous solution and at room temperature. This chemical behavior is due to various interactions of PolyNaSS-SH with gold facets [110] based on their different degree of polymerization and their steric conformation of chemical groups during nucleation and growth process of AuNPs. Contrary to previous methods,²¹ the gold core was protected with a cross-linked polymer shell, inhibiting the dissociation of linear polymer brushes from the nanoparticles

at room temperature. The absorption spectra of PolyNaSS-SH@AuNPs (5, 10, and 35 kDa) were characterized by a small peak at 310 nm, assigned to the PolyNaSS-SH absorption (5 and 10 kDa), and a surface plasmon band at 541 nm for PolyNaSS-SH@AuNPs (5 kDa) (Figure 1, black line) and 546 nm for PolyNaSS-SH@AuNPs (10 kDa) due to a major degree of polymerization onto gold nanoparticles (Figure 1, red line) in which we observed a disappearance of the peak at 310 nm due to a different steric conformation of the polymer onto AuNPs. The different spectroscopic behavior was observed in the presence of PolyNaSS-SH@AuNPs (35 kDa) in which we observed a decrease of the UV–vis spectrum intensity (Figure 1, blue line) and a blue shift of around 10 nm of the LPS band (from 541 to 534 nm). This phenomenon could be ascribed to the change of localized refractive index and morphology, indicating that the PolyNaSS-SH was differently coordinated to the AuNP surface. It is generally acknowledged that the peak intensity and position of the LPS band depend on the size and shape of AuNPs.⁸ Based on the UV–vis spectrum of PolyNaSS-SH@AuNPs, we assumed that such a spectroscopic behavior could be associated to the successful functionalization of the AuNP surface with PolyNaSS-SH. We assumed that, during the synthesis process, there are different collision rates of PolyNaSS-SH-Au micelles, which depend on the size of the macromolecular chains (M_n from 5 to 35 kDa). This effect is responsible of the variation of the NPs' final shape due to a probable deposition of PolyNaSS-SH molecules onto Au facet [110]. Moreover, it is noteworthy that PolyNaSS-SH can be used as a stabilizing polymer for AuNPs due to the formation of coordination bands between the Au ions and the sulfonate and carboxylic groups of PolyNaSS-SH. This chelation provokes a better dispersion of the Au ions, which are more easily reduced to form single AuNPs of relatively uniform size. This behavior is associated to $\pi-\pi^*$ electronic transitions due to the interactions between the aromatic ring and AuCl_4^- ions, giving clear evidence of the complex formation.⁷ In addition, the color bright pink violet of both nanoparticles and the UV–

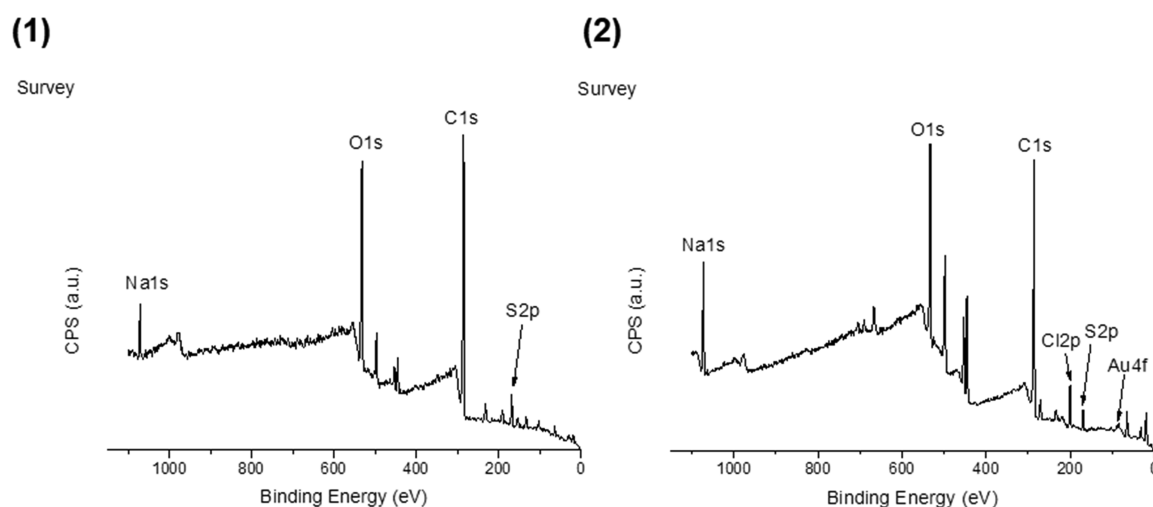


Figure 2. XPS survey spectra for (1) PolyNaSS-SH 35 kDa powder and (2) PolyNaSS-SH@AuNPs (35 kDa).

vis spectra remain unaltered after storage for more than 6 months at room temperature, suggesting the formation of stable particle suspension (test stability, see Figure S1). DLS and zeta potential measurements show that PolyNaSS-SH@AuNPs were colloidally stable at physiological pH (ζ -potential = -25 ± 1 mV; ζ -potential = -27 ± 1 mV and -30 ± 1 mV with PDI = 0.3) regardless of the molecular weights of 5, 10, or 35 kDa (Figure S13 in the Supporting Information). This stability was enhanced with the presence of the PolyNaSS coating. The steric arrangement of PolyNaSS-SH during the synthetic process of gold nanoparticles was confirmed by Raman spectroscopic analysis (Figure 1). In detail, Raman spectra of PolyNaSS-SH@AuNPs exhibited several bands in the region of 200–1500 cm^{-1} (Figure 1-2). PolyNaSS-SH@AuNPs (5 kDa; Figure 1-2, black line) showed only a few bands at 796 and 623 cm^{-1} due to C–H plane deformation and a broadened peak at 452 cm^{-1} assigned to the vibrations δ (OH...O) and ν (OH...O) of the PolyNaSS-SH in aqueous solution. These bands were due to variation of the steric conformation of the PolyNaSS-SH and became more prominent upon complexation with AuCl_2^- .

In fact, when C=O and hydroxyl groups of PolyNaSS-SH interact with a metal, the sterical conformation became more tilted with respect to the planar one. Indeed, in the case of PolyNaSS-SH@AuNPs (10 kDa ($n = 48$); Figure 1-2, red line), a new peak appeared at 232 cm^{-1} , confirming a plane active deformation of the polymer. The gold chloride stretches ν (Au–Cl) and δ (O–Au–O), corroborating the formation of a complex between the AuCl_2^- and COOH group of PolyNaSS-SH in the solution. Improving the number of polymerization, from $n = 48$ (10 kDa) to 170 (35 kDa), we observed an SERS effect and apportioned a double peak at 348–278 cm^{-1} due to a different steric arrangement and complexation of PolyNaSS with AuCl_4^- (PolyNaSS-SH@AuNPs (35 kDa); Figure 1-2, blue line). Based on the previous studies,⁷ we assumed that Au^{3+} ions promoted the deprotonation of the carboxylic group.

2.2.1. XPS Characterization of the PolyNaSS-SH Powder and PolyNaSS-SH@AuNPs. The first set of data presents the spectra acquired for the powder. One can see on the survey spectrum in Figure 2(1) the presence of all features expected for the PolyNaSS-SH compound, namely, carbon (C 1s @ 285 eV), oxygen (O 1s @ 530 eV), sulfur (S 2p @ 170 eV), and

the sodium counterion (Na 1s @ 1080 eV). Apart from qualitative analyses, XPS data can also be used for quantitative analyses. However, due to the high degree of polymerization ($M_n = 35$ kDa), only data from the polymeric part could be analyzed. Table 1A summarizes the different atomic percent-

Table 1. (A) Atomic Percentages for both the PolyNaSS-SH Powder and PolyNaSS-SH@AuNPs. (B) O 1s Atomic Percentages for both the PolyNaSS-SH Powder and PolyNaSS-SH@AuNPs

A	condition	C 1s (%)	O 1s (%)	S 2p (%)	Na 1s (%)	Au 4f
PolyNaSS-SH Powder 35 kDa	theoretical	61.5	23.1	7.7	7.7	
	experimental	68.7	23.65	5.0	2.65	
PolyNaSS-SH@AuNPs (35 kDa)	theoretical	61.5	23.1	7.7	7.7	N/A
	experimental	66.55	22.4	4.3	6.55	0.2
B		O 1s (%)				
BE		535.8	533.3	531.6		
PolyNaSS-SH Powder 35 kDa		1.12	5.7	16.6		
PolyNaSS-SH@AuNPs (35 kDa)		2.0	2.1	18.9		

ages obtained from XPS compared to the theoretical ones. Both sets of data are rather in good agreement, except for a slight overexpression of the carbon atomic percentage, which is usually observed when analyzing powder deposited on indium foil as it was the case here. Experimental O 1s and S 2p percentages were rather closed to the theoretical expected ones with nonetheless a huge difference for the Na 1s. This last point is observed quite often and could be explained by the fact that the complexation of the counterion in the PolyNaSS-SH molecule was not followed until the equilibrium and/or went away after the different rinsing procedures.²⁴ When looking at the ratio S 2p/O 1s, the theoretical one is 0.33, while the calculated ratio is 0.21, as shown in Table 1.

However, when looking at the different contributions used for the decomposition of the whole O 1s signal, one should take into account that only the low binding energy component at 531.4 eV (Figure 2) is assigned to the SO_3^- moiety. Therefore, Table 1B shows the percentage of the three O 1s components, and the ratio S 2p/O 1s_{531.4eV} is 0.30, which

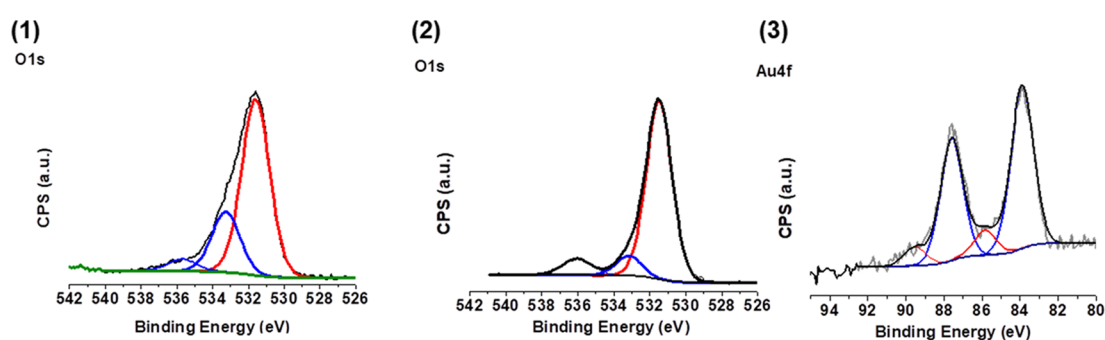


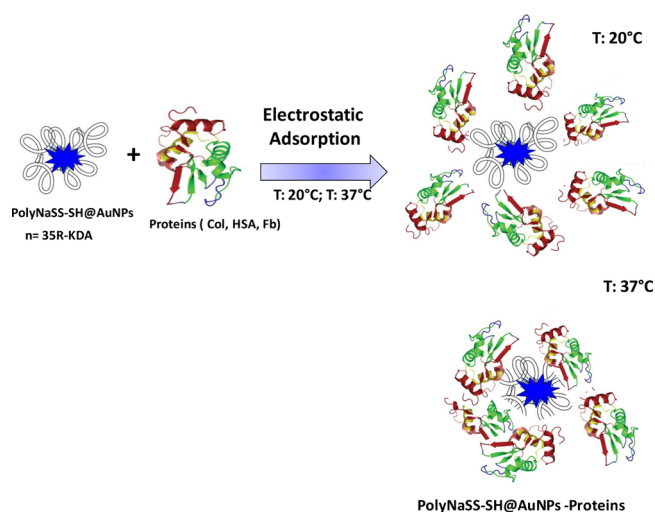
Figure 3. XPS O 1s high-resolution region spectra for (1) PolyNaSS-SH powder 35 kDa, (2) PolyNaSS-SH@AuNPs (35 kDa), and (3) XPS Au 4f high-resolution region spectrum for PolyNaSS-SH@AuNPs (35 kDa).

correlates very well with the theoretical/expected one. The second set of experiments was performed on the gold nanoparticles synthesized using PolyNaSS-SH powder as a stabilizing agent. The survey spectrum is shown in Figure 2(2) where one can see an additional feature at 84.0 eV corresponding to the Au 4f signal, together with the previous signal of PolyNaSS-SH observed previously in Figure 2(1). Again, all experimental atomic percentages are shown in Table 1 and fit correctly with the expected theoretical values for PolyNaSS-SH. One can note the very small amount of gold detected, only 0.2%, but is explained again by the thickness of the outer shell of PolyNaSS-SH of the highest molecular weight. The S 2p/O 1s 531.4 eV ratio is even lower than the theoretical one of 0.22 in the case of PolyNaSS-SH-AuNPs, which could be due to an excess of an aqueous solvent when drying the AuNP solution for the XPS analyses. Finally, when looking more specifically to the Au 4f region in Figure 3(3), one can see the presence of two sets of doubles, one centered at 84.0 eV for the Au 4f_{7/2} (86.8%) assigned to metallic gold (Au⁰) and a second one at around 86.0 eV (13.2%) assigned to Au³⁺. This result suggests that the reaction was not the total and that a small portion of ionic gold remained in the solution. It also confirmed by the presence of some Cl 2p signal at 200 eV (Figure 2-2).

2.3. Interactions of PolyNaSS-SH@AuNPs (35 kDa) with Human Proteins. Migonney *et al.* established that the distribution of the anionic groups along the macromolecular chains of PolyNaSS creates active sites, which can specifically interact with the extracellular matrix proteins (ECM) such as fibronectin (Fn) and collagen I (Col 1) that are implicated in the cell response.^{12,20} The mechanism at the origin of these activities comes from the presence of the sulfonate groups of PolyNaSS, which allows the mimicking of glycosaminoglycane and modulating protein adsorption.²⁰ Here, we realized a preliminary study of the interaction between plasmatic proteins such as human serum albumin (HSA), Col 1, and Fn with PolyNaSS-SH@AuNPs (35 kDa) (Scheme 2) by using UV-vis absorption and Raman spectroscopy (pH = 7.2, 20 °C, and 37 °C). All proteins were observed to adsorb onto PolyNaSS-SH-AuNPs (35 kDa) through van der Waals and electrostatic interactions. The time of corona formation was estimated at 24 h, and the protein concentration was around 1 μM.

2.3.1. Col 1 Adsorption. Col is an abundant natural protein with several applications in medicine mainly as a scaffold for tissue engineering applications.²⁵ Figure 5A shows a localized plasmonic band (LPB) of PolyNaSS-SH@AuNPs (35 kDa) before and after Col adsorption at room temperature (RT) (20 °C). The observed decrease in the plasmonic band against Col

Scheme 2. Schematic Representation of the Interactions between the PolyNaSS-SH@AuNP (35 kDa) Flower core-shell and Human Proteins at Temperatures of 20 and 37 °C Conditions



concentration was attributed to the adsorption process of Col onto AuNPs at RT. This was confirmed by the Raman spectra (Figure 4A1) in which we can observe a disappearance of the peak at 886 cm⁻¹ due to ν (C–C) (D-(+)-galactosamine) and the appearance of the peak at 1121 cm⁻¹ due to the C–H bending of proteins.²⁶

The adsorption of Col onto PolyNaSS-SH@AuNPs (35 kDa) at 37 °C showed a similar behavior of the LPB band at 1 μM concentration (Figure 4B). The major difference was observed in Raman spectra in which, at 1 μM collagen, a strong spectral modification appeared due to the peaks at 264, 324, 453, and 613 cm⁻¹ attributed to the vibrations δ (OH...O), ν (OH...O), ν_4 (δ) PO₄³⁻, and ν_2 (δ) PO₄³⁻ doubly degenerate in-plane bending vibrations. The appearance of a double peak at 990–1030 cm⁻¹ and a peak at 1453 cm⁻¹ confirms a change of conformation of the protein onto PolyNaSS-SH@AuNPs (35 kDa) due to CH₂ deformation, carbohydrate phosphate, and phenylalanine ring breathing²⁶ (Figure 4B1). When comparing the collagen interaction in the presence of PolyNaSS-SH@AuNPs (5 kDa), we observed an identical spectroscopic behavior at the two T conditions (20 and 37 °C) (Figure S14A-A1,B-B1). After Col adsorption, the Raman spectroscopy displayed the appearances of novel peaks at 327, 445, and 620 cm⁻¹ due to the vibrations δ (OH...O), ν (OH...O), ν_4 (δ) PO₄³⁻, and ν_2 (δ) PO₄³⁻ and a double peak at

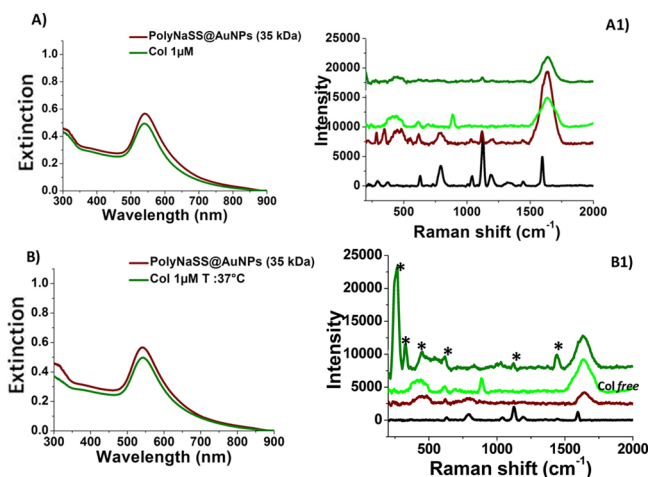


Figure 4. (A, B) Normalized UV-vis absorption spectra of PolyNaSS-SH@AuNPs (35 kDa) before (purple line) and after interaction of collagen (Col I) (1 μM) (green cyan line) at (A) 20 and (B) 37 $^{\circ}\text{C}$. (A1, B1) Raman spectra of PolyNaSS-SH@AuNPs before (purple line) and after interaction of collagen (Col) (1 μM) (green cyan line) at (A1) 20 and (B1) 37 $^{\circ}\text{C}$ PolyNaSS-SH (35 kDa, black line) and Col I free (green line) was added as control. Experimental conditions: $\lambda_{\text{exc}} = 785 \text{ nm}$; laser power, 20 mW; accumulation time, 180 s.

1034–996 cm^{-1} due to CH_2 deformation. This demonstrates the difference of Col conformation when adsorbed on PolyNaSS-SH@AuNPs (35 kDa) compared to PolyNaSS-SH@AuNPs (5 kDa).

2.3.2. HSA Adsorption. In the case of HSA,¹⁸ the LPB band at room temperature showed a decrease of the absorption intensity from 530 to 545 nm for 1 μM concentration with a decrease of the peak at 310 nm, confirming the partial interaction of the protein with the NPs (Figure S15A).

The Raman spectra of HSA free showed a peak at 437 cm^{-1} and a double peak at 296–328 cm^{-1} due to the plane active deformation of protein.²⁷ In accordance with previous works,¹⁴ the spectra were dominated by amide II and III vibrations at 1559 and 1250 cm^{-1} , respectively, and by the bands assigned to vibrations of aromatic amino acid side chains such as their ring vibrations at 630 cm^{-1} . In our case, the amide band of HSA was masked by water in a region of 1680 cm^{-1} . The presence of the stretching vibrations of S–S bonds at 437 cm^{-1} ²⁸ in HSA suggests that the protein molecules maintain

their disulfide bridges as important elements of their secondary structure upon interaction with the nanoparticle surface.²⁸

The Raman spectra double peak at 296–328 cm^{-1} disappears, and a peak at 1080–1127 cm^{-1} due to the ring stretching of tryptophan²⁹ or the deformation vibrations of the $-\text{NH}_2$ group at 1512, 1058, and at 1070 cm^{-1} ³⁰ appears (Figure S15B). The latter two bands also contained contributions of vibrations $\text{C}\alpha-\text{N}$ and $\text{C}-\text{CH}_2$ bonds in the peptide backbone, in accordance with a distinct signal of the $\text{C}-\text{N}$ stretching band at 1170 cm^{-1} . The enhancement of the SERS signals from the $-\text{NH}_2$ groups and of the protein backbone indicates the proximity of the basic amino acid residues and of the peptide backbone, respectively, to the nanoparticle. The several bands of HSA in Raman spectra assigned to aromatic and aliphatic vibrations indicate their proximity to the nanoparticle surface, which could also point toward a hydrophobic interaction with the nanoparticles. The basic amino (NH_2) groups can be expected to interact with the sulfonate (SO_3^-) group in an acid–base equilibrium. After 24 h at 37 $^{\circ}\text{C}$ (Figure S15B1), a shoulder peak at 1620 cm^{-1} was observed in the presence of nanoparticles. This peak was attributed to a local change of extended and side chains. In opposite of behavior at RT, the LPB band in UV-vis showed an increase of the absorption peak after the HSA interaction is proportional to protein concentration. Contrary to Col I, the interactions between HSA and PolyNaSS-SH@AuNPs (5 kDa) did not display any spectroscopic modification under experimental conditions. This observation was expected since HSA is a nonspecific protein that adsorbs onto all polymer surfaces without any specificity, which is not the case of Col I (Figure S16).

This different behavior of Col I is similar to HSA on two NP surfaces of different composition (35 vs 5 kDa), confirming the chemical relationship between specific protein and length of the grafted polymer onto AuNPs. On the basis of this result, we assume that the best candidate to control the interaction of proteins is PolyNaSS-SH@AuNPs (35 kDa).

2.3.3. Fn Adsorption. The study of the adsorption of Fn onto PolyNaSS-SH@AuNPs (35 kDa) was achieved at 37 $^{\circ}\text{C}$ only due to the sensitivity of this large protein toward temperature and to prevent its precipitation.³¹ Fn is a high molecular weight adhesive glycoprotein, which is composed of two large macromolecular chains (250 kDa) that are linked by disulfide bonds at their carboxy-terminal ends.³² Figure 5 shows a weak blue shift of the LPB band from 540 to 535 nm with a disappearance of the peak at 310 nm, attributed to Fn

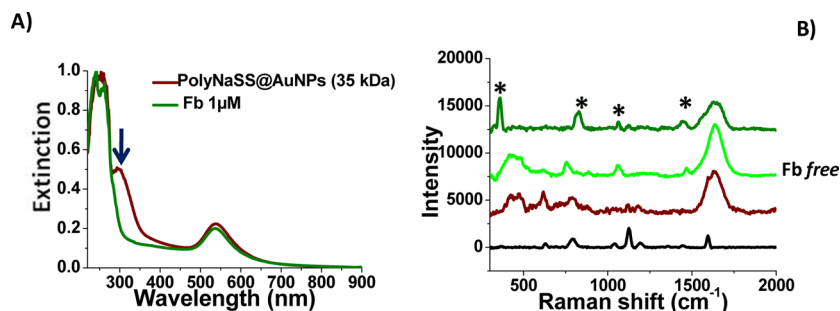


Figure 5. (A, B) Normalized UV-vis absorption spectra of PolyNaSS-SH@AuNPs (35 kDa) before (purple line) and after interaction of fibronectin (Fn) (1 μM) (green cyan line) at 37 $^{\circ}\text{C}$. (B) Raman spectra of PolyNaSS-SH@AuNPs before (purple line) and after interaction of fibronectin (Fn) (1 μM) (green cyan line) PolyNaSS-SH (35 kDa, black line) and Fn free (green line) was added as control. Experimental conditions: $\lambda_{\text{exc}} = 785 \text{ nm}$; laser power, 20 mW; accumulation time, 180 s.

adsorption onto PolyNaSS-SH@AuNPs (35 kDa). The interaction of Fn onto PolyNaSS grafted onto surfaces was previously demonstrated to be specific, confirming that the observed interactions of Fn onto PolyNaSS-SH@AuNPs lead to a particular conformation/orientation of the protein. The adsorption of Fn on PolyNaSS-SH@AuNPs (35 kDa) was confirmed by Raman spectra in which we observed that, after the interaction with Fn (1 μ M), a peak appeared at 437 cm^{-1} due to the plane active deformation of protein and several peaks at 900, 1300, and 1490 cm^{-1} corresponding to Fn.³³ The peak at 1448 cm^{-1} can be assigned to the deformation modes of both CH_3 and CH_2 vibrations. The 1424 cm^{-1} band is a COO stretching mode where the amide III band occurs. The sharp band at 1001 cm^{-1} belongs to phenylalanine (ring breathing mode). Fn adsorbs specifically on PolyNaSS functionalized NPs.

2.4. Selectivity of Proteins onto PolyNaSS-SH@AuNPs (35 kDa). To confirm the selectivity of protein adsorption onto PolyNaSS-SH@AuNPs (35 kDa), a preliminary test was carried out in the presence of Col I and citrate AuNPs as a negative control. Col I solution (from 1 μ M and 100 nM) was incubated with citrate AuNPs at 37 $^\circ\text{C}$, and the interaction/adsorption was monitored by UV-vis and Raman spectroscopy. Figure S17 shows remarkable precipitation of colloidal solution (citrate AuNPs) after protein interaction without spectroscopical modification. This means that there was no capture of the Col I at the citrate AuNP surface even at a high concentration of protein. We thus conclude that the PolyNaSS-SH@AuNP surface selectively interacts with Col I under physiological conditions.

3. CONCLUSIONS

This study could be employed in the field of regenerative nanomedicine to improve the osteointegration and hope that a novel view will be suggested for the development of hybrid nanomaterials. In summary, we conceive a fast original methodology to obtain core-shell flower shape hybrid nanoparticles in a one-step synthesis, tuning the degree of polymerization of PolyNaSS-SH with significantly improved stability. The hybrid nanomaterials obtained showed a different chemical behavior after interaction with human plasmatic proteins. Indeed, we assume that the nature of the protein as well as the temperature of the adsorption influences the interactions of proteins with PolyNaSS-SH@AuNPs. The better interactions between protein and NPs occur at 37 $^\circ\text{C}$, which corresponds to the physiologic temperature. On the basis of these conclusions, we can provide further cytotoxicity assays and cell interaction studies as perspectives. To the best of our knowledge, these aspects have never been described before in published reports.

4. EXPERIMENTAL SECTION

All the reagents were provided by the Sigma-Aldrich chemical company and received unless otherwise specified. Sodium styrene sulfonate (NaSS) was recrystallized in an ethanol/water mixture (9/1, v/v).¹⁴ ^1H NMR spectra were recorded on a Bruker Avance III (400 MHz) or a Bruker Avance III (500 MHz) spectrometer in D_2O at 300 K. The H_2O signal (δ 4.79 ppm) is used as the internal reference. The average molecular weight (M_n) of PolyNaSS was obtained by aqueous size exclusion chromatography (SEC), as previously described.¹⁶ Briefly, the mobile phase consisted of 0.1 mL min^{-1} sodium

nitrate aqueous solution. Analyses were carried out at 40 $^\circ\text{C}$ with a flow rate of 0.5 mL min^{-1} . Calibration was realized with a monodisperse PolyNaSS standard (MW 4800–75,600), purchased from Sigma-Aldrich.

4.1. Determination of Monomer Conversion. Monomer conversion (x) was calculated from ^1H NMR data using the following equation

$$x = \frac{(\int Ht = 0) - (\int Htf)}{(\int Ht = 0)} \quad (1)$$

$\int Ht = 0$ and $\int Htf$ are the integration of one of vinyl proton from monomer at the beginning (t_0) and the end (t_f) of RAFT polymerization, respectively, by setting the integral of the solvent peak at 1.

4.2. Calculation of the Theoretical Molecular Weight of Polymer (M_{nth}). The theoretical average molecular weight (M_{nth}) of PolyNaSS samples was determined using the following equation (eq 2)

$$M_{\text{nth}} = \frac{[\text{monomer}]_0}{[\text{RAFT agent}]} \times x \times M_{\text{monomer}} + M_{\text{RAFT}} \quad (2)$$

$[\text{monomer}]_0$ and $[\text{RAFT agent}]$ are the initial monomer concentration and initial RAFT agent concentration, respectively. x is monomer the conversion, and M_{monomer} and M_{RAFT} are the molecular weight of monomer and RAFT agent, respectively.

4.3. RAFT Polymerization of NaSS. The synthesis of PolyNaSS by RAFT polymerization was carried out following the procedure previously described in the literature.¹⁶ For the general procedure for the polymerization in water, 4,4'-azobis(4-cyanovaleric acid) and 4-cyano-4-(phenylcarbonothioylthio)pentanoic acid were used as the initiator and transfer agent, respectively. NaSS (5 g, 2.43 $\cdot 10^{-2}$ mol) was dissolved in 15 mL of water, and the amount of transfer agent was exactly adjusted to obtain the desired M_n of polymers. Solutions were degassed under argon at room temperature (RT) for 20 min. Polymerizations were carried at 70 $^\circ\text{C}$ for 5 h and stopped by rapid cooling. The product was precipitated into 350 mL of ice-cold methanol. After overnight drying under vacuum at 50 $^\circ\text{C}$, PolyNaSS samples were analyzed by ^1H NMR.

4.4. SH End Group Formation of PolyNaSS-SH by Reduction Reaction. PolyNaSS (4 g) were dissolved in 10 mL of water and degassed under argon for 15 min. Then, 10 mL of deoxygenated sodium borohydride aqueous solution (NaBH_4 ; 1 M) and 2 mL of tributylphosphine (PBu_3) were added to the polymer solution and kept bubbling under argon for 15 min. The solution was stirred for at least 48 h at room temperature (RT) before the PolyNaSS-SH was precipitated in ice-cold methanol. After this time, PolyNaSS-SH was filtered and washed with methanol to remove residual NaBH_4 . After drying overnight under vacuum at 50 $^\circ\text{C}$, the PolyNaSS-SH powder samples were dissolved in 600 μL of D_2O and analyzed by ^1H NMR. The ratio of the thiol and carboxylic acid to styrene sulfonate is different: for the 5 kDa PolyNaSS, we obtained 24 sulfonate functions for 1 thiol function and 1 carboxylic acid, for the 10 kDa PolyNaSS, we obtained 48 sulfonate functions for 1 thiol and 1 carboxylic acid, and for the 35 kDa PolyNaSS, we obtained 169 sulfonate functions for 1 thiol and 1 carboxylic acid.

4.5. ¹H NMR Analysis of PolyNaSS and PolyNaSS-SH.

PolyNaSS 5 kDa, ¹H NMR (500 MHz, D₂O) δ (ppm): 8.15–7.28 (m, 2H); 7.20–6.12 (m, 2H); 2.07–0.87 (m, 3H); PolyNaSS 10 kDa, ¹H NMR (500 MHz, D₂O) δ (ppm): 8.08–7.27 (m, 2H); 7.20–6.08 (m, 2H); 2.07–0.83 (m, 3H); PolyNaSS 35 kDa, ¹H NMR (500 MHz, D₂O) δ (ppm): 7.80–7.22 (m, 2H); 7.08–6.12 (m, 2H); 2.07–0.877 (m, 3H); PolyNaSS-SH 5 kDa, ¹H NMR (500 MHz, D₂O) δ (ppm): 7.78–7.23 (m, 2H); 6.98–6.08 (m, 2H); 1.99–1.02 (m, 3H); PolyNaSS-SH 10 kDa, ¹H NMR (500 MHz, D₂O) δ (ppm): 7.78–7.23 (m, 2H); 6.98–6.08 (m, 2H); 1.99–1.02 (m, 3H); PolyNaSS-SH 35 kDa, ¹H NMR (500 MHz, D₂O) δ (ppm): 7.78–7.23 (m, 2H); 6.98–6.08 (m, 2H); 1.99–1.02 (m, 3H); PolyNaSS-SH@AuNPs (5 kDa), ¹H NMR (500 MHz, D₂O) δ (ppm): 7.88–7.14 (m, 2H); 7.05–6.05 (m, 2H); 2.00–0.94 (m, 3H); PolyNaSS-SH@AuNPs (10 kDa), ¹H NMR (500 MHz, D₂O) δ (ppm): 7.88–7.14 (m, 2H); 7.05–6.05 (m, 2H); 2.00–0.94 (m, 3H); PolyNaSS-SH@AuNPs (35 kDa), ¹H NMR (500 MHz, D₂O) δ (ppm): 7.88–7.14 (m, 2H); 7.05–6.05 (m, 2H); 2.00–0.94 (m, 3H).

4.6. Synthesis of PolyNaSS-SH@AuNPs (PolyNaSS-SH:

5 kDa; 10kDa; 35 kDa). Aqueous HAuCl₄ solution (20 mL, 0.8 mM) was mixed with 5 mL of PolyNaSS-SH (5, 10, and 5 kDa) solution (1 g/20 mL) at room temperature (RT) for 20 min under stirring to form a Au-PolyNaSS-SH complex. Then, 1.5 mL of NaBH₄ (1 and 5 mM) was added, rapidly stirred and kept without agitation for 2 h. In the first step, the color of the dispersion changed from green yellow (HAuCl₄ solution) to pink red when PolyNaSS-SH (5, 10, and 35 kDa) was complexed with gold salt. Finally, when sodium borohydride was added to a solution of PolyNaSS-SH gold precursor, a reduction of metal ions confirms the formation of hybrid nanoparticles in the solution with a characteristic purple color. The as-prepared PolyNaSS-SH@AuNPs solution was purified by centrifugation and dialysis to remove excess of not-conjugated PolyNaSS-SH.

4.7. Interaction of PolyNaSS-SH@AuNPs (M_n 35 kDa) with Proteins. The interaction of PolyNaSS-SH@AuNPs (M_n 35 kDa) with human proteins (Col, HSA, Fn) were achieved following the procedures depicted in Scheme 2. Briefly, 900 μL of PolyNaSS-SH@AuNPs (35 kDa) (1 mM) were added into separate tubes containing 100 μL of each protein at three different concentrations (10–100 nM and 1 μM, PBS pH 7, and NaCl 0.15 M). After 20 h of incubation, at 20 or 37 °C, the NPs/protein suspension was centrifuged twice at 5000 rpm for 10 min to eliminate the nonadsorbed protein; then, the pellets were resuspended in 1 mL of Milli-Q water.

4.8. Determination of PolyNaSS-SH@AuNP Concentration. PolyNaSS-SH@AuNP concentration was established by mathematical calculations in colloidal solution. The Lambert–Beer law ($A = \epsilon Cl$) was applied to define colloid concentration, as previously described.³⁴

4.9. Physicochemical Characterization. All the measurements were performed in triplicate to validate the reproducibility of the synthetic and analytical procedures as described previously.^{8,9}

4.9.1. XPS Analysis. XPS analyses were performed using an Omicron Argus X-ray photoelectron spectrometer, equipped with a monochromated Al K α radiation source ($h\nu = 1486.6$ eV) and a 300 W electron beam power. The emission of photoelectrons from the sample was analyzed at a takeoff angle of 90° under ultrahigh vacuum conditions ($\leq 10^{-10}$ Torr). Spectra were carried out with 100 eV pass energy for the

survey scan and 20 eV pass energy for the C 1s, O 1s, Na 1s, S 2p, and Au 4f regions. Binding energies were calibrated against the C 1s binding energy at 284.8 eV, and element peak intensities were corrected by Scofield factors.³⁵ The spectra were fitted using the CasaXPS v.2.3.15 software (Casa Software Ltd., U.K.) and applying a Gaussian/Lorentzian ratio (G/L) equal to 70/30; otherwise stated, Shirley-type backgrounds were used.

■ ASSOCIATED CONTENT

Supporting Information

The Supporting Information is available free of charge at <https://pubs.acs.org/doi/10.1021/acsomega.0c00376>.

Stability test (Figure S1); functional assignment of peaks and intensity of infrared spectra of PolyNaSS (Table S1); infrared spectra of PolyNaSS-SH (5, 10, 35 kDa) grafting onto AuNPs (Figure S2); H NMR analysis (Figure S3 to S9); GPC analysis (Figures S10 to S12 and Table S2); DLS analysis (Figure S13); interaction human proteins (Figures S14 to S17) (PDF)

■ AUTHOR INFORMATION

Corresponding Author

Jolanda Spadavecchia – CNRS, UMR 7244, NBD-LBPS-CSPBAT, Laboratoire de Chimie, Structures et Propriétés de Biomateriaux et d'Agents Thérapeutiques Université Paris 13, 93000 Bobigny, France; orcid.org/0000-0001-6697-1174; Email: jolanda.spadavecchia@univ-paris13.fr

Authors

Céline Falentin-Daudré – CNRS, UMR 7244, NBD-LBPS-CSPBAT, Laboratoire de Chimie, Structures et Propriétés de Biomateriaux et d'Agents Thérapeutiques Université Paris 13, 93000 Bobigny, France; orcid.org/0000-0002-5526-6194

Mounia Aitouakli – CNRS, UMR 7244, NBD-LBPS-CSPBAT, Laboratoire de Chimie, Structures et Propriétés de Biomateriaux et d'Agents Thérapeutiques Université Paris 13, 93000 Bobigny, France

Jean Sébastien Baumann – CNRS, UMR 7244, NBD-LBPS-CSPBAT, Laboratoire de Chimie, Structures et Propriétés de Biomateriaux et d'Agents Thérapeutiques Université Paris 13, 93000 Bobigny, France

Nadia Bouchemal – CNRS, UMR 7244, NBD-LBPS-CSPBAT, Laboratoire de Chimie, Structures et Propriétés de Biomateriaux et d'Agents Thérapeutiques Université Paris 13, 93000 Bobigny, France

Vincent Humblot – FEMTO-ST Institute, UMR CNRS 6174, Université Bourgogne Franche-Comté, 25030 Besançon, France; orcid.org/0000-0002-6266-3956

Véronique Migonney – CNRS, UMR 7244, NBD-LBPS-CSPBAT, Laboratoire de Chimie, Structures et Propriétés de Biomateriaux et d'Agents Thérapeutiques Université Paris 13, 93000 Bobigny, France; orcid.org/0000-0002-1055-3720

Complete contact information is available at: <https://pubs.acs.org/doi/10.1021/acsomega.0c00376>

Notes

The authors declare no competing financial interest.

■ ACKNOWLEDGMENTS

We acknowledge the NMR-PF facility (University Paris 13 France).

REFERENCES

- (1) Gentile, A.; Ruffino, F.; Grimaldi, M. Complex-Morphology Metal-Based Nanostructures: Fabrication, Characterization, and Applications. *Nanomaterials* **2016**, *6*, 110.
- (2) Zhang, Y.; Cui, X.; Shi, F.; Deng, Y. Nano-Gold Catalysis in Fine Chemical Synthesis. *Chem. Rev.* **2012**, *112*, 2467–2505.
- (3) Lee, H. K.; Lee, Y. H.; Koh, C. S. L.; Phan-Quang, G. C.; Han, X.; Lay, C. L.; Sim, H. Y. F.; Kao, Y.-C.; An, Q.; Ling, X. Y. Designing surface-enhanced Raman scattering (SERS) platforms beyond hotspot engineering: emerging opportunities in analyte manipulations and hybrid materials. *Chem. Soc. Rev.* **2019**, *48*, 731–756.
- (4) Sukhanova, A.; Bozrova, S.; Sokolov, P.; Berestovoy, M.; Karaulov, A.; Nabiev, I. Dependence of Nanoparticle Toxicity on Their Physical and Chemical Properties. *Nanoscale Res. Lett.* **2018**, *13*, 44–44.
- (5) Lin, Y. C.; Tan, F. J.; Marra, K. G.; Jan, S. S.; Liu, D. C. Synthesis and characterization of collagen/hyaluronan/chitosan composite sponges for potential biomedical applications. *Acta Biomater.* **2009**, *5*, 2591.
- (6) Dipankar, C.; Murugan, S. The green synthesis, characterization and evaluation of the biological activities of silver nanoparticles synthesized from Iresine herbstii leaf aqueous extracts. *Colloids Surf., B* **2012**, *98*, 112.
- (7) Moustaoui, H.; Movia, D.; Dupont, N.; Bouchemal, N.; Casale, S.; Djaker, N.; Savarin, P.; Prina-Mello, A.; de la Chapelle, M. L.; Spadavecchia, J. Tunable Design of Gold(III)–Doxorubicin Complex–PEGylated Nanocarrier. The Golden Doxorubicin for Oncological Applications. *ACS Appl. Mater. Interfaces* **2016**, *8*, 19946–19957.
- (8) Spadavecchia, J.; Apchain, E.; Albéric, M.; Fontan, E.; Reiche, I. One-step synthesis of collagen hybrid gold nanoparticles and formation on Egyptian-like gold-plated archaeological ivory. *Angew. Chem., Int. Ed.* **2014**, *53*, 8363–8366.
- (9) Spadavecchia, J.; Movia, D.; Moore, C.; Maguire, C. M.; Moustaoui, H.; Casale, S.; Volkov, Y.; Prina-Mello, A. Targeted polyethylene glycol gold nanoparticles for the treatment of pancreatic cancer: from synthesis to proof-of-concept in vitro studies. *Int. J. Nanomed.* **2016**, *11*, 791–822.
- (10) Monteil, M.; Moustaoui, H.; Picardi, G.; Aouidat, F.; Djaker, N.; de La Chapelle, M. L.; Lecouvey, M.; Spadavecchia, J. Polyphosphonate ligands: From synthesis to design of hybrid PEGylated nanoparticles toward phototherapy studies. *J. Colloid Interface Sci.* **2018**, *513*, 205–213.
- (11) Ding, T.; Lu, W. W.; Zheng, Y.; Li, Z. Y.; Pan, H. B.; Luo, Z. Rapid repair of rat sciatic nerve injury using a nanosilver-embedded collagen scaffold coated with laminin and fibronectin. *Regener. Med.* **2011**, *6*, 437.
- (12) Helary, G.; Noirclere, F.; Mayingi, J.; Migonney, V. A new approach to graft bioactive polymer on titanium implants: Improvement of MG 63 cell differentiation onto this coating. *Acta Biomater.* **2009**, *5*, 124–133.
- (13) Felgueiras, H. P.; Decambron, A.; Manassero, M.; Tulasne, L.; Evans, M. D. M.; Viateau, V.; Migonney, V. Bone tissue response induced by bioactive polymer functionalized Ti6Al4V surfaces: In vitro and in vivo study. *J. Colloid Interface Sci.* **2017**, *491*, 44–54.
- (14) Chouirfa, H.; Migonney, V.; Falentin-Daudré, C. Grafting bioactive polymers onto titanium implants by UV irradiation. *RSC Adv.* **2016**, *6*, 13766–13771.
- (15) Chouirfa, H.; Evans, M. D. M.; Bean, P.; Saleh-Mghir, A.; Crémieux, A. C.; Castner, D. G.; Falentin-Daudré, C.; Migonney, V. Grafting of Bioactive Polymers with Various Architectures: A Versatile Tool for Preparing Antibacterial Infection and Biocompatible Surfaces. *ACS Appl. Mater. Interfaces* **2018**, *10*, 1480–1491.
- (16) McCormick, C. L.; Lowe, A. B. Aqueous RAFT polymerization: recent developments in synthesis of functional water-soluble (co)-polymers with controlled structures. *Acc. Chem. Res.* **2004**, *37*, 312–325.
- (17) Falentin-Daudré, C.; Baumann, J.-S.; Migonney, V.; Spadavecchia, J. Highly crystalline sphere and rod-shaped TiO₂ nanoparticles: A facile route to bio-polymer grafting. *Front. Lab. Med.* **2017**, *1*, 217–223.
- (18) Shao, Q.; Hall, C. K. Allosteric effects of gold nanoparticles on human serum albumin. *Nanoscale* **2017**, *9*, 380–390.
- (19) Saptarshi, S. R.; Duschl, A.; Lopata, A. L. Interaction of nanoparticles with proteins: relation to bio-reactivity of the nanoparticle. *J. Nanobiotechnol.* **2013**, *11*, 26–26.
- (20) Chouirfa, H.; Evans, M. D. M.; Castner, D. G.; Bean, P.; Mercier, D.; Galtayries, A.; Falentin-Daudré, C.; Migonney, V. Grafting of architecture controlled poly(styrene sodium sulfonate) onto titanium surfaces using bio-adhesive molecules: Surface characterization and biological properties. *Biointerphases* **2017**, *12*, No. 02C418.
- (21) Dong, H.; Zhu, M.; Yoon, J. A.; Gao, H.; Jin, R.; Matyjaszewski, K. One-Pot Synthesis of Robust Core/Shell Gold Nanoparticles. *J. Am. Chem. Soc.* **2008**, *130*, 12852–12853.
- (22) Jena, B. K.; Raj, C. R. Synthesis of Flower-like Gold Nanoparticles and Their Electrocatalytic Activity Towards the Oxidation of Methanol and the Reduction of Oxygen. *Langmuir* **2007**, *23*, 4064–4070.
- (23) Kang, Y.; Taton, T. A. Core/Shell Gold Nanoparticles by Self-Assembly and Crosslinking of Micellar, Block-Copolymer Shells. *Angew. Chem., Int. Ed.* **2005**, *44*, 409–412.
- (24) Amokrane, G.; Humblot, V.; Jubeli, E.; Yagoubi, N.; Ramtani, S.; Migonney, V.; Falentin-Daudré, C. Electrospun Poly(*ε*-caprolactone) Fiber Scaffolds Functionalized by the Covalent Grafting of a Bioactive Polymer: Surface Characterization and Influence on in Vitro Biological Response. *ACS Omega* **2019**, *4*, 17194–17208.
- (25) Chattopadhyay, S.; Raines, R. T. Review collagen-based biomaterials for wound healing. *Biopolymers* **2014**, *101*, 821–833.
- (26) Bakker Schut, T. C.; Caspers, P. J.; Puppels, G. J.; Nijssen, A.; Heule, F.; Neumann, M. H. A.; Hayes, D. P. Discriminating Basal Cell Carcinoma from its Surrounding Tissue by Raman Spectroscopy. *J. Invest. Dermatol.* **2002**, *119*, 64–69.
- (27) Plank, J. Applications of biopolymers and other biotechnological products in building materials. *Appl. Microbiol. Biotechnol.* **2004**, *66*, 1–9.
- (28) Rygula, A.; Majzner, K.; Marzec, K. M.; Kaczor, A.; Pilarczyk, M.; Baranska, M. Raman spectroscopy of proteins: a review. *J. Raman Spectrosc.* **2013**, *44*, 1061–1076.
- (29) Madzharova, F.; Heiner, Z.; Kneipp, J. Surface Enhanced Hyper-Raman Scattering of the Amino Acids Tryptophan, Histidine, Phenylalanine, and Tyrosine. *J. Phys. Chem. C* **2017**, *121*, 1235–1242.
- (30) Lin, V. J. C.; Koenig, J. L. Raman studies of bovine serum albumin. *Biopolymers* **1976**, *15*, 203–218.
- (31) Raoufi, M.; Hajipour, M. J.; Kamali Shahri, S. M.; Schoen, I.; Linn, U.; Mahmoudi, M. Probing fibronectin conformation on a protein corona layer around nanoparticles. *Nanoscale* **2018**, *10*, 1228–1233.
- (32) Pankov, R.; Yamada, K. M. Fibronectin at a glance. *J. Cell Sci.* **2002**, *115*, 3861–3863.
- (33) Strehle, M. A.; Rösch, P.; Petry, R.; Hauck, A.; Thull, R.; Kiefer, W.; Popp, J. A Raman spectroscopic study of the adsorption of fibronectin and fibrinogen on titanium dioxide nanoparticles. *Phys. Chem. Chem. Phys.* **2004**, *6*, 5232–5236.
- (34) Liu, Q.; Sacco, P.; Marsich, E.; Furlani, F.; Arib, C.; Djaker, N.; Lamy de la Chapelle, M.; Donati, I.; Spadavecchia, J. Lactose-Modified Chitosan Gold(III)-PEGylated Complex-Bioconjugates: From Synthesis to Interaction with Targeted Galectin-1 Protein. *Bioconjugate Chem.* **2018**, *29*, 3352–3361.
- (35) Scofield, J. H. Hartree-Slater subshell photoionization cross-sections at 1254 and 1487 eV. *J. Electron Spectrosc. Relat. Phenom.* **1976**, *8*, 129–137.